Journal of
Materials Chemistry C

ROYAL SOCIETY OF CHEMISTRY

COMMUNICATION

View Article Online
View Journal | View Issue

Check for updates

Cite this: *J. Mater. Chem. C*, 2023, **11**, 1265

Received 11th November 2022,
Accepted 28th December 2022

DOI: 10.1039/d2tc04802g

rsc.li/materials-c

A circularly polarized (CP) white organic light-emitting diode (WOLED) based on a chiral organo-Sm^{3+} complex†

Jiaxiang Liu,‡[a] Baowen Wang,‡[a] Zhiming Zhang,[a] Jiamiao Yu,[a] Xingqiang Lü, *[a]
Guorui Fu,*[a] Wentao Li*[ab] and Wai-Yeung Wong *[b]

Using the designed chiral [Sm(tta)$_3$(D-phen)] as an emitter, the first example of a chiral organo-Ln^{3+}-based CP-WOLED with both attractive white-light efficiencies (η_{EQE}^{Max} = 1.55% and η_{CE}^{Max} = 1.61 cd A^{-1}) and high dissymmetry factor ($|g_{EL}|^{Max}$ = 0.011) is reported.

Inspired by the direct generation of circularly polarized light (CPL), CP-OLEDs (organic light-emitting diodes)[1] capable of high-contrast 3D images and true backlight, are significantly superior to traditionally unpolarized OLEDs.[2] In this perspective, to realize efficient CP electroluminescence, concerted efforts have been devoted to the development of different chiroptical luminophores, such as chiral organic small-molecules,[3] chiral conjugated polymers,[4] chiral metal (transition[5]/lanthanide[6]) complexes as well as chiral thermally active delayed fluorescent (TADF) emitters.[7] In consideration of a restriction of theoretical 25% internal quantum efficiency (η_{IQE})[3,4] for chiral small-molecules and conjugated polymers with fluorescence, chiral metal complexes[5,6] and TADFs[7] enable the harvesting of both ^{1}S and ^{1}T excitons, which makes the resulting phosphorescent CP-OLEDs with η_{IQE}^{Max} = 100% more appealing. Nonetheless, it remains a great challenge to achieve satisfactory polarization degree and high device efficiency, simultaneously. On the other hand, accompanying the attractive high-performance with monochrome (visible and even near-infrared (NIR)) features of the reported CP-OLEDs,[1] the realization of reliable panchromatic or white CP-OLEDs (CP-WOLEDs) is very rare and in its infancy.[8] For instance, although the current efficiency (η_C^{Max}, 2.0–50.0 cd A^{-1}) of the reported CP-WOLEDs fabricated from chiral *bis*-benzoxanethone fluorescent emitters by Cheng *et al.*[8a] or spiro-type TADFs by Zheng *et al.*[8b] is high enough for portable full-colour 3D displays ($\eta_C^{Max} > 0.5$ cd A^{-1}),[9] one issue of their inferior white-light quality (CIE coordinates 0.32–0.35, 0.45–0.46) still occurs, probably arising from the dichromatic and voltage-dependent white-light integrations.[10] Additionally, their intrinsically low polarization degree is also difficult to solve.

As a matter of fact, CPL activity quantified by the dissymmetry factor g_{lum} (corresponding to photo-excited g_{PL} or electric-driven g_{EL}) *via* the following equation[11] originates from the intensity (I_L or I_R) difference of the emissive left and right CP lights. Meanwhile, from the viewpoint of quantum mechanics, g_{lum} can further be simplified to be relative to the electric (μ) and magnetic (m) transition dipole moments and the θ angle between.

$$g_{lum} = 2\frac{I_L - I_R}{I_L + I_R} = 4\frac{|m| \cdot |\mu|}{|m|^2 + |\mu|^2} \cos\ \theta$$

For most chiral organic luminophores (small-molecules, TADFs and polymers, *etc.*) or chiral transition-metal complexes, their relatively small $|g_{PL}|$ values in the $10^{-5} \sim 10^{-4}$ range,[12] are attributed to the high μ and the negligible m sizes. In contrast, uniquely beneficial from the magnetically allowed while electrically forbidden f–f transitions of the Ln^{3+} ion, distinctively higher $|g_{PL}|$ values ($> 10^{-2}$), especially for Eu^{3+}, Tb^{3+} or Sm^{3+} ions, are found for their chiral organo-Ln^{3+} complexes.[13] For example, chiral Cs[Eu((+/−)-hfbc)$_4$][14] (**hfbc** = 3-heptafluoro-butylyrylcamphorate) showed the highest $|g_{PL}|$ of 1.38 among the reported CPL-active materials[12,13] so far, and by using them as dopants, smart examples of visible-monochromatic (Eu^{3+}-centred colour-purity red-light) CP ($|g_{EL}|$ = 0.15–1.00) devices[14,15] have been realized. However, arising from the (+/−)-hfbc-induced unsatisfactory photoluminescence efficiency (Φ_{PL}, < 2%), the subsequent standstill is reflected in their very low maximal external quantum efficiency (η_{EQE}^{Max}, 4.2 × 10^{-3} − 0.05%) even with light out-coupling technology. Recently, through a modular design strategy to chiral [Eu(tta)$_3$(*R*/*S*-PyBox)] (**Htta** = thenoyltrifluoroacetone; **PyBox** = pyridine *bis*-oxazoline) complexes,[16] the **Htta**-induced triplet state ^{1}T compatible with the first excited state (^{5}D$_0$) of Eu^{3+} ions was

---

[a] *School of Chemical Engineering, Northwest University, Xi'an 710069, Shaanxi, China. E-mail: lvxq@nwu.edu.cn, fuguorui@nwu.edu.cn*
[b] *Department of Applied Biology and Chemical Technology, Research Institute for Smart Energy, The Hong Kong Polytechnic University, Hung Hom, Hong Kong, China. E-mail: wentaowh.li@polyu.edu.hk, wai-yeung.wong@polyu.edu.hk*

† Electronic supplementary information (ESI) available: Starting materials and characterization; UV; PL. See DOI: https://doi.org/10.1039/d2tc04802g

‡ These authors contributed equally and should be considered co-first authors.

demonstrated to give desirably improved ($\eta_{\text{EQE}}^{\text{Max}}$ = 0.48% and $|g_{\text{EL}}|$ = 0.51) Eu^{3+}-red-light CP-OLEDs. However, along with no other visible-monochromatic CP-OLED reports from chiral organo-Tb^{3+}/Sm^{3+} systems, the outward field of chiral organo-Ln^{3+}-based CP-WOLEDs, to the best of our knowledge, is also not reported. Noticeably, contributed from the unique f–f transitions, the Eu^{3+}/Tb^{3+}/Sm^{3+}-centred high-purity (red/green/orange) primary colour is relatively fixed, and receives much less interference from external stimulations (such as ligand-field, pH, temperature, concentration, photo-excitation or electric-driving, *etc.*).[17] Therefore, despite great efforts towards white-light emitters[18] with desirable g_{PL} sizes, chiral organo-Eu^{3+}/Tb^{3+}/Sm^{3+} complexes should offer a conceptual opportunity for CP-WOLEDs. Moreover, in comparison to the chiral non-Ln^{3+}-dye counterparts,[8] the salient advantages of their white-light stability and high CPL-activity could be expected during photo-excitation and/or electric-driving.

Encouraged by the progressive advance of organo-Eu^{3+}/Tb^{3+}/Sm^{3+}-colour-primary OLEDs[19] or white-light emitters,[20] it is of significance to explore the state-of-the-art chiroptical activity of chiral organo-Eu^{3+}/Tb^{3+}/Sm^{3+} complexes toward desirable CP-WOLEDs while not monochromatic CP-OLEDs.[14–16] Considering the simplification of white-light modulation[21] from a dichromatic while not typical trichromatic (RGB) strategy, herein, one efficient chiral organo-Sm^{3+} complex **[Sm(tta)$_3$(D-phen)]** (see Scheme 1) is molecularly designed. The conception points include: (i) besides the lower triplet state (^{1}T) energy of **Htta** than that of **D-phen**, the compatibility between the ^{1}T of **Htta** and the first excited state ($^4G_{5/2}$) of the Sm^{3+} ion should engender efficient and high-purity orange-light for **[Sm(tta)$_3$(D-phen)]**; (ii) motivated by the higher $|g_{\text{lum}}|$ while shorter lifetime values of organo-Sm^{3+} complexes than those of the corresponding organo-Eu^{3+}/Tb^{3+} counterparts in some cases,[13] strong CPL-activity and relatively low efficiency-roll-off from **[Sm(tta)$_3$(D-phen)]** can be expected; (iii) most importantly, keeping Sm^{3+}-centred stable and high-purity orange-light at hand and further using the popular blue-emitting PVK (poly(*N*-vinylcarbazole) as the colour-compensated host for low-cost solution-processed device fabrication, the targeted **[Sm(tta)$_3$(D-phen)]**-doped CP-WOLED ruled by the blue-orange dichromatic principle, could be realized. And thus, this present research, to the best of our knowledge, is the first example of chiral organo-Ln^{3+}-based CP-WOLEDs.

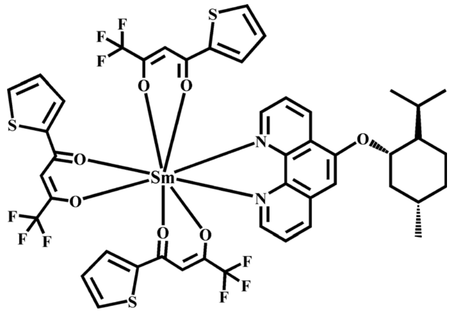

Scheme 1 Structural scheme of the designed chiral organo-Sm^{3+} complex **[Sm(tta)$_3$(D-phen)]**.

The chiral **Phen** (phenanthroline) derivative **D-phen** was synthesized in a higher yield (72% *versus* 65%) according to the improved synthetic procedure (Scheme S1, ESI†) for **2-L-Phen** by the stronger Lewis-base KH instead of NaH as in the literature.[22] Following the full characterization by EA, FT-IR and ^{1}H NMR (ESI†), its chiroptical activity was further checked to afford $[\alpha]_D^{25}$ = 56.0 ± 0.1°, which almost resembled that ($[\alpha]_D^{25}$ = 50°) of (+)-menthol, showing the retention of the original absolute configuration. Also as shown in Scheme S1 (ESI†), further through the self-assembly of the chiral ancillary **D-phen** with the complex precursor [Ln(tta)$_3$(H$_2$O)] (Ln = Sm or La),[23] the corresponding chiral organo-Ln(III) complex **[Sm(tta)$_3$(D-phen)]** or **[La(tta)$_3$(D-phen)]** was obtained as the iso-structural product, respectively. The two chiral complexes **[Sm(tta)$_3$(D-phen)]** and **[La(tta)$_3$(D-phen)]** soluble in common organic solvents except water, were well characterized by EA, FT-IR, ^{1}H NMR and ESI-MS (see ESI†). In particular, based on the ^{1}H NMR spectrum (Fig. 1) of anti-magnetic[24] counterpart **[La(tta)$_3$(D-phen)]**, the signals (δ = 9.57–0.75 ppm) of both **(tta)$^-$** and **D-phen** proton resonances were identified, respectively, which together with a stipulated 3 : 1 molar ratio, well confirms its desirable binary tris-(β-diketonate)-La^{3+} component. Meanwhile, as compared with the free **Htta** (δ = 7.83–6.45 ppm), the high-field shifts of all the proton signals (δ = 7.54–6.14 ppm) to the coordinated **(tta)$^-$** ligands were observed. However, in contrast to the free **D-phen** (δ = 9.17–0.78 ppm), the aromatic proton resonances (δ = 9.57–6.93 ppm) of the coordinated **D-phen** within were significantly low-field shifted, which, also upon La^{3+} coordination, should be the reason for the broadened proton resonances (δ = 9.57–0.75 ppm) of **[La(tta)$_3$(D-phen)]**. The thermogravimetric analysis (TGA) result (see Fig. S1, ESI†) shows that **[Sm(tta)$_3$(D-phen)]** has similar thermal stability to **[La(tta)$_3$(D-phen)]**, and the decomposition (5 wt% loss) temperature of about 300 °C is sufficient for the following device fabrication.

The optical properties of the chiral complex **[Sm(tta)$_3$(D-phen)]** in solution were explored at room temperature, and

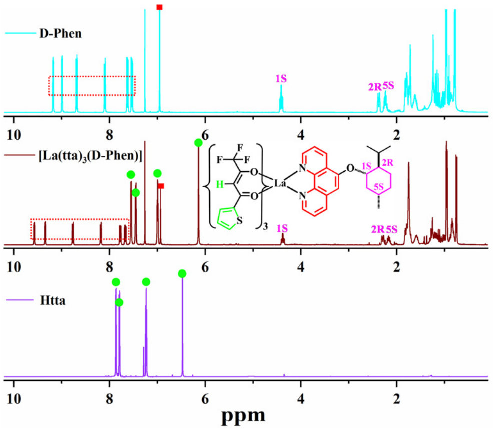

Fig. 1 ^{1}H NMR spectra of the free ligands **Htta** and **D-phen**, and their chiral complex **[La(tta)$_3$(D-phen)]** in $CDCl_3$ at room temperature, respectively.

the results are summarized in Fig. 2. In contrast to the UV-visible absorptions of the free ligands (229, 244, 271 and 314 nm for **D-phen**, 262 and 329 nm for **Htta**; Fig. S2, ESI†), the ligand-centred while significantly red-shifted (229, 246, 284 and 330 nm; see Fig. 2(a)) absorption bands of the chiral complex **[Sm(tta)$_3$(D-phen)]** are observed, due to the Sm^{3+}-coordination. Upon photo-excitation, λ_{ex} within the 230–420 nm range just renders the Sm^{3+}-centred emissions for the chiral complex **[Sm(tta)$_3$(D-phen)]**, as shown in Fig. 2(b), where the splitting λ_{em} = 565, 595, 643 and 711 nm, corresponding to $^4G_{5/2} \rightarrow {}^6H_{J/2}$ (J = 5, 7, 9, 11) transitions of Sm^{3+} ion, are assigned, correspondingly. Noticeably, the highest intensity (λ_{em} = 643 nm) is at the hypersensitive $^4G_{5/2} \rightarrow {}^6H_{9/2}$ transition and the lowest one (λ_{em}= 711 nm) from the $^4G_{5/2} \rightarrow {}^6H_{11/2}$ transition, meaning that the central Sm^{3+} ion is located in a site without inversion symmetry.[25] Meanwhile, apart from the absence of the ligand-centred emissions, the integration of the two electric dipole (μ) transitions above and the other two $^4G_{5/2} \rightarrow {}^6H_{7/2}$ and $^4G_{5/2} \rightarrow {}^6H_{5/2}$ magnetic dipole (m) transitions (λ_{em} = 565 and 595 nm), engenders a bright colour-purity orange-light with the CIE (Commission International De L'Eclairage) coordinates of x = 0.604, y = 0.371. Moreover, its outstanding photoluminescence is further reflected from the attractive Φ_{PL} of *ca.* 10% in the solid-state, which is almost comparable to that[26] of non-chiral complex [Sm(tta)$_3$(Phen)]. Furthermore, the decay lifetime of the Sm^{3+}-centred (λ_{em} = 643 nm) transition for the chiral complex **[Sm(tta)$_3$(D-phen)]** is 72 μs, distinctively shorter than those (10^2 μs grade) of typical tris-(β-diketonate)-Eu^{3+}/Tb^{3+} complexes,[27] and thus, it renders an additional opportunity for relatively weak efficiency-roll-off during device application.

To deeply understand the photo-physical behaviour of the chiral complex **[Sm(tta)$_3$(D-phen)]**, TD-DFT (time-dependent density functional theory) calculations of the *anti*-magnetic chiral complex **[La(tta)$_3$(D-phen)]** counterpart for simplification were carried out, and the details are summarized in Tables S1, S2 (ESI†) and Fig. 3. As shown in Fig. 3, similar domination from three (**tta**)$^-$ ligands to each of the HOMOs (12.16/32.47/53.96% for the HOMO; 50.03/12.54/36.06% for the HOMO−1; 36.65/53.02/7.88% for the HOMO−2), and the most contribution (85.05%) also from three (**tta**)$^-$ ligands in non-equivalent mode (33.60/45.47/5.96%) to the LUMO+1 is observed. However, a substantial proportion (12.67%) from the **D-phen** ligand to the LUMO+1 cannot be neglected, which is different from the minor ones to all the HOMOs. As to the LUMO or the LUMO+2, it is mostly localized at the chiral **D-phen** unit (94.64% *versus* 86.37%). Through the calculated HOMO → LUMO transition (388 nm) dominated for the $S_0 \rightarrow S_1$ excitation, the experimentally determined low-energy (over 330 nm; also see Fig. 2(a)) should mainly be attributed to the ^{1}LLCT (LLCT = ligand-to-ligand charge transfer; (**tta**)$^-$ to **D-phen**) transition. Accordingly, besides the HOMO–LUMO energy of 3.69 eV, a theoretical first excited state level (^{1}T; $^3\pi$–π^*) of 2.453 eV (19802 cm^{-1}) can further be calculated. By checking the energy level match between the $^3\pi$–π^* and the $^4G_{5/2}$ (17 064 cm^{-1}) of the Sm^{3+} ion, a suitable energy gap ΔE (2738 cm^{-1}) within the ideal 2500–4000 cm^{-1} range according to the so-called Latva's empirical rule,[28] reasonably confirms the effective sensitization (see Fig. S3, ESI†) of Sm^{3+} ions. Therefore, not relevant to the chirality but beneficial to the strengthened absorption of **D-phen**, the efficient and colour-purity Sm^{3+}-centred orange-light for its chiral complex **[Sm(tta)$_3$(D-phen)]** is understandable.

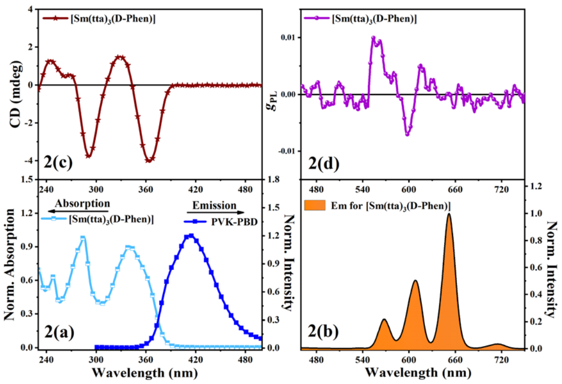

Fig. 2 (a) Normalized absorption of chiral **[Sm(tta)$_3$(D-phen)]** in solution and emission of PVK-PBD (65 : 30; weight ratio) in the solid-state (λ_{ex} = 273 nm); (b) emission, (c) CD or (d) CPL spectra of chiral **[Sm(tta)$_3$(D-phen)]** in solution at room temperature, respectively.

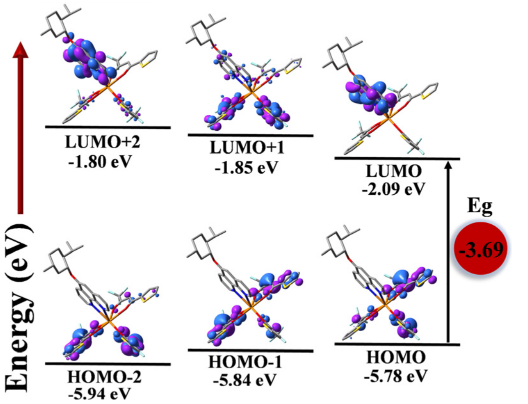

Fig. 3 The HOMO and LUMO patterns for the chiral complex **[Sm(tta)(D-phen)]** based on its optimized S_0 geometry, respectively.

The chiroptical properties including CD (circular dichroism; also see Fig. 2(c)) and CPL (see Fig. 2(d)) spectra of the chiral complex **[Sm(tta)$_3$(D-phen)]** in solution were studied. As shown in Fig. 2(c), the evident CD signals are exhibited, indicative of the chirality retention[29] upon complex formation. And in contrast to the Cotton-effect bands (Fig. S4 (ESI†); (+)-231, (−)-246, (+)-267 and (+)-312 nm) of **D-phen**, the significantly red-shifted Cotton-effect ones at (+)-245, (−)-291, (+)-327 and (−)-365 nm arising from the Sm^{3+}-coordination are observed for the chiral complex **[Sm(tta)$_3$(D-phen)]**. In particular, the low-energy Cotton-effect absorption can be assigned to the exciton-coupled CT transition. Upon photo-excitation, as shown in Table S3 (ESI†) and Fig. 2(d), the typically Sm^{3+}-centred CPL spectrum of the chiral complex **[Sm(tta)$_3$(D-phen)]** was exhibited, where based on the corresponding $^4G_{5/2} \rightarrow {}^6H_{7/2}$ and $^4G_{5/2} \rightarrow {}^6H_{5/2}$ magnetic dipole (m) allowed transitions, the largest g_{PL} of +0.009 is detected at λ_{em} = 560 nm ascribed to the $^4G_{5/2} \rightarrow {}^6H_{5/2}$ transition. It is worth noting that the D-**phen**-ancillary $|g_{PL}|^{Max}$ value (0.009) is relatively lower than those (0.10–1.15; $|g_{PL}|$) of the previous chiral organo-Sm^{3+} complexes[30] with chirality from the N^O/O^O main ligands, whilst their $^3\pi$–π^* energies are too high to effectively sensitize the Sm^{3+}-centred orange-light. On the other hand, besides the top level of the $|g_{PL}|$ = 0.009 among those of the reported chiral organo-Sm^{3+}complexes with chirality from the ancillary ligands,[31] the (**tta**)$^-$-incorporation leads to the attractive Φ_{PL} (*ca.* 10%) for its high-purity orange-light. Importantly, the uniquely CPL-active property is unreachable from chiral non-organo-Ln^{3+} sources ($|g_{PL}|$ values within the $10^{-5}\sim10^{-4}$-grade),[32] despite the more efficient while non-high-purity orange-light.

Considering the strong CPL activity and high-purity orange-light arising from the chiral complex **[Sm(tta)$_3$(D-phen)]**, it is of special interest for low-cost solution-processed CP-WOLEDs. Through its doping into the commercial electron-transporting PBD (2-(4-tert-butylphenyl)-5-(4-biphenyl)-1,3,4-oxadiazole) and the hole-transporting PVK mixture (5 : 30 : 65, weight ratio) as the EML (emitting layer), the colour-integration with blue-light (also see Fig. 2(a)) from the bipolar PVK-PBD host and the orange-light from **[Sm(tta)$_3$(D-phen)]** should be compensated forward to a desirable CP white-light. In particular, besides an effective Förster energy transfer[33] confirmed from the significant spectral overlap (also see Fig. 2(a)) between the emission of PVK-PBD and the CT absorption of **[Sm(tta)$_3$(D-phen)]**, its experimentally obtained HOMO/LUMO energies (−5.40/−2.17 eV; CV as Fig. S5, ESI†) fall well within those (−5.80/−2.16 eV) of PVK-PBD, making PVK-PBD a suitable bipolar host. Profiting from a peculiar stepwise alignment of the HOMO/LUMO levels from the EML to TPBi (−6.20/−2.70 eV; further facilitating electron-transport) and to BCP (−6.70/−3.20 eV; hole-blocking), the carrier-balancing device with ITO/PEDOT:PSS (40 nm)/EML (80 nm)/TPBi (30 nm)/BCP (10 nm)/LiF (1 nm)/Al (100 nm) was configured (see Fig. 4(a and b)).

As expected, upon illumination with the turn-on voltage (V_{on} at 1 cd m^{-2}) of 7.0 V, the normalized electroluminescent spectra (Fig. 4(c)) in the applied bias voltage range of 7.0–13.0 V exhibit the simultaneous emissions of the host-based blue-light (λ_{em} = 424 nm) and the Sm^{3+}-centred orange-light ($^4G_{5/2} \rightarrow {}^6H_{J/2}$ (J = 5, 7, 9, 11) transitions). Noticeably, although the dichromatic colour-integration with CIE coordinates x = 0.268–0.297, y = 0.203–0.224 is highly dependent on the applied bias voltage (see Table S4, ESI†), all the emissive colours fall well within the desirable white-light regime. Moreover, all the warm-white-lights, endowing the CRIs (colour render indices) of 96–97 and the CCTs (correlated colour temperatures) of 2625–2631 K, mostly integrated from Sm^{3+}-characteristic orange-light, are relatively stable. Among them, the minor colour-coordinate shifts ($|\Delta x|$ = 0.029 and $|\Delta y|$ = ≤ 0.021) with different blue-to-orange relative intensity ratios should probably be due to doping-induced phase-separation of the EML. As shown in Fig. 4(d and e), in contrast to the monotonous increase of the current density (J, mA cm^{-2}) or the luminance (L, cd m^{-2}) with increasing the applied bias voltage, all the efficiencies (η_C (current efficiency; cd A^{-1})), η_P (power efficiency; lm W^{-1}) and η_{EQE} (external quantum efficiency)) increase instantly and then decrease steadily throughout the whole illumination with the η_C^{Max} = 1.61 cd A^{-1}, the η_P^{Max} = 0.59 lm W^{-1} and the η_{EQE}^{Max} = 1.55% at 8.5 V (L = 3.86 cd m^{-2}), respectively. Even at a practical luminance of 100 cd m^{-2}, the considerable efficiencies (η_C^{Max} = 1.09 cd A^{-1}, η_P^{Max} = 0.36 lm W^{-1} and η_{EQE}^{Max} = 1.03%) can be maintained, from which, the efficiency-roll-offs of 32–39% are acceptable. Intriguingly, as shown in Table S5 (ESI†) and Fig. 4(f), the sizable dissymmetric factor $|g_{EL}|^{max}$ of 0.011 at λ_{em} = 560 nm ($^4G_{5/2} \rightarrow {}^6H_{5/2}$ transition of Sm^{3+} ion) is kept.

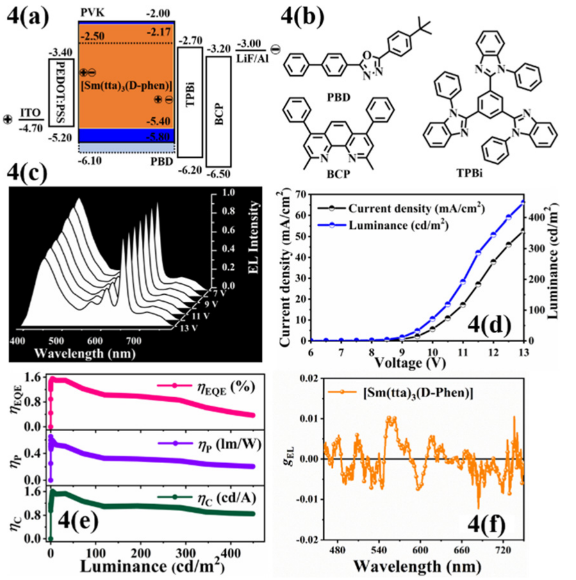

Fig. 4 (a) Device structure and energy level diagram; (b) molecular structures of PBD, BCP and TPBi; (c) electroluminescent spectra; (d) J–V and L–V curves; (e) η_{EQE}–L, η_P–L and η_C–L curves; (f) g_{EL}–λ_{EL} curve for the **[Sm(tta)$_3$(D-phen)]**-doped CP-WOLED, respectively.

As compared with those (η_C^{Max}, 2.0–50.0 cd A^{-1}; $|g_{EL}| \sim 10^{-3}$) of the reported CP-WOLEDs from chiral *bis*-benzoxanethone[8a] or spiro-type TADFs,[8b] the η_C^{Max} = 1.61 cd A^{-1} of the **[Sm(tta)$_3$(D-phen)]**-doped CP-WOLED is relatively lower while satisfactory enough to that (η_C^{Max} > 0.5 cd A^{-1}) for portable full-colour 3D displays.[9] Undoubtedly, one of the merits for the **[Sm(tta)$_3$(D-phen)]**-doped CP-WOLED rests with the $|g_{EL}|$ size increased by one order of magnitude. More importantly, another evident advantage lies in the high-quality and stable white-lights mainly integrated with the Sm^{3+}-centred orange-light. On the other hand, the device performance of the **[Sm(tta)$_3$(D-phen)]**-doped CP-WOLED is also at the top-level among those (η_C^{Max} = 0.65–4.90 cd A^{-1}) of the previously reported WOLEDs[34] from non-chiral organo-Sm^{3+} dyes (Φ_{PL}= 5.6–8.1%). Saliently, the higher-efficiency (η_C^{Max} = 1.61 cd A^{-1} and η_{EQE}^{Max} = 1.55%) should inherently benefit from the improved Φ_{PL} up to 10% from **[Sm(tta)$_3$(D-phen)]**. In the meantime, relying on the PBD/TPBi-facilitated electron-transport, more effective carrier confinement and recombination in the EML should be in a subordinate position. Furthermore, upon a stepwise alignment[35] of the HOMO/LUMO levels combined with the BCP-interface blocking, the desirable carrier balance might take into effect and especially benefit the relatively weak efficiency-roll-offs.

In conclusion, through the incorporation of the enantiopure **D-phen** as the ancillary, its chiral complex **[Sm(tta)$_3$(D-phen)]** displaying both efficient (Φ_{PL} = 10%) Sm^{3+}-centred colour-purity orange-light and strong CPL activity (g_{PL} = 0.009; $^4G_{5/2} \rightarrow {}^6H_{5/2}$ transition) was molecularly designed. Moreover, by using the chiral complex **[Sm(tta)$_3$(D-phen)]** as the dopant, the resulting CP-WOLED (η_{CE}^{Max} = 1.61 cd A^{-1}) and $|g_{EL}|^{Max}$ = 0.011) was successfully developed. Noticeably, this research work, as the first example of chiral organo-Ln^{3+}-based CP-WOLEDs, suggests that chiral organo-Sm^{3+}/Eu^{3+}/Tb^{3+} complexes should be promising candidates for portable 3D full-colour displays.

Conflicts of interest

There are no conflicts to declare.

Acknowledgements

This work was supported by the NSFC (21373160, 21173165, 51873176, 22201229), the Young Elite Scientists Sponsorship Program by the Association of Shaanxi Science and Technology (20220405), the Hong Kong Research Grants Council (PolyU153058/19P), the CAS-Croucher Funding Scheme for Joint Laboratories (ZH4A), the Hong Kong Polytechnic University (1-ZE1C and YW4T), Research Institute for Smart Energy, and the Endowed Professorship in Energy from Ms Clarea Au (847S).

Notes and references

1 (*a*) D. W. Zhao, M. Li and C. F. Chen, *Chem. Soc. Rev.*, 2020, **49**, 1331–1343; (*b*) J. M. Han, S. Guo, H. Lu, S. J. Liu, Q. Zhao and W. Huang, *Adv. Opt. Mater.*, 2018, **6**, 1800538; (*c*) D. Steiger and C. Weder, *Opt. Sci. Eng.*, 2007, **111**, 451–481.

2 (*a*) B. Van de Zee, Y. G. Li, G.-J. A. H. Wetzelaer and P. W. M. Blom, *Adv. Mater.*, 2022, **34**, 2108887; (*b*) J. Song, H. Lee, E. G. Jeong, K. C. Kyund and S. Yoo, *Adv. Mater.*, 2020, **32**, 1907539; (*c*) X. L. Yang, G. J. Zhou and W.-Y. Wong, *Chem. Soc. Rev.*, 2015, **44**, 8484–8575; (*d*) B. J. Powell, *Coord. Chem. Rev.*, 2015, **295**, 46–79; (*e*) H. Sasabe and J. Kido, *J. Mater. Chem. C*, 2013, **1**, 1600–1707.

3 (*a*) Y. Chen, *Mater. Today Chem.*, 2022, **23**, 100651; (*b*) J. L. Ma, Q. Peng and C. H. Zhao, *Chem. – Eur. J.*, 2019, **25**, 15441–15454; (*c*) J. Kumar, T. Nakashima and T. Kawai, *J. Phys. Chem. Lett.*, 2015, **6**, 3445–3452.

4 Y. T. Sang, J. L. Han, T. H. Zhao, P. F. Duan and M. H. Liu, *Adv. Mater.*, 2020, **32**, 1900110.

5 B. Doistau, J.-R. Jimenez and C. Piguet, *Front. Chem.*, 2020, **8**, 555.

6 F. Zinna and L. Di Bari, *Chirality*, 2015, **23**, 3721–3730.

7 L. Zhou, G. H. Xie and C. L. Yang, *Appl. Phys. Lett.*, 2020, **117**, 130502.

8 (*a*) Y. Zhang, J. Li, Y. W. Quan, S. H. Ye and Y. X. Cheng, *Chem. – Eur. J.*, 2021, **27**, 589–593; (*b*) Y. P. Zhang, M. X. Miao, S. Q. Song, Y. Wang, Y. X. Zheng, J. L. Zuo and Y. Pan, *Angew. Chem., Int. Ed.*, 2022, **61**, e202200290.

9 A. de Bettencourt-Dias, *Dalton Trans.*, 2007, 2229–2241.

10 (*a*) Z. Chen, C.-L. Ho, L. Q. Wang and W.-Y. Wong, *Adv. Mater.*, 2020, **32**, 1903269; (*b*) G. M. Farinola and R. Ragni, *Chem. Soc. Rev.*, 2011, **40**, 3467–3482; (*c*) M. C. Gather, A. Koehnen and K. Meerholz, *Adv. Mater.*, 2011, **23**, 233–248.

11 L. Arrico, L. Di Bari and F. Zinna, *Chem. – Eur. J.*, 2021, **27**, 2920–2934.

12 (*a*) L. Zhang, H. X. Wang, S. Li and M. H. Liu, *Chem. Soc. Rev.*, 2020, **49**, 9095–9120; (*b*) G. Yang, C. Ren, X. D. Lin and T. C. He, *Front. Chem.*, 2020, **8**, 458.

13 H.-Y. Wong, W.-S. Lo, K.-H. Yim and G.-L. Law, *Chemistry*, 2019, **5**, 3058–3095.

14 F. Zinna, U. Giovanella and L. Di Bari, *Adv. Mater.*, 2015, **27**, 1791–1795.

15 F. Zinna, M. Pasini, F. Galeotti, C. Botta, L. Di Bari and U. Giovanella, *Adv. Funct. Mater.*, 2017, **27**, 1603719.

16 F. Zinna, L. Arrico, T. Funaioli, L. Di Bari, M. Pasini, C. Botta and U. Giovanella, *J. Mater. Chem. C*, 2022, **10**, 463–468.

17 S. V. Eliseeva and J.-C.-G. Bünzli, *Chem. Soc. Rev.*, 2010, **39**, 189–227.

18 (*a*) M. R. Han, H. T. Zhang, J. N. Wang, S. S. Feng and L. P. Lu, *RSC Adv.*, 2019, **9**, 32288–32295; (*b*) W. B. Wang, R. Y. Wang, Y. F. Ge and B. L. Wu, *RSC Adv.*, 2018, **8**, 42100–42108; (*c*) X. Ma, X. Li, Y. E. Cha and L. P. Jin, *Cryst. Growth Des.*, 2012, **12**, 5227.

19 (*a*) L. D. Wang, Z. F. Zhao, C. Wei, H. B. Wei, Z. W. Liu, Z. Q. Bian and C. H. Huang, *Adv. Opt. Mater.*, 2019, **7**, 1801256; (*b*) M. A. Katkova and M. N. Bochkarev, *Dalton Trans.*, 2010, **39**, 6599–6612; (*c*) J. Kido and Y. Okamoto, *Chem. Rev.*, 2002, **102**, 2357–2368.

20 (*a*) T. Tang, H. L. Wu, W. Q. Cao, Y. J. Cui and G. D. Qian, *Adv. Opt. Mater.*, 2021, **9**, 2001817; (*b*) S. SeethaLekshmi, A. R. Ramya, M. L. P. Reddy and S. Varughese, *J. Photochem. Photobiol., C*, 2017, **33**, 109–131.

21 M. Pan, W. M. Liao, S. Y. Yin, S. S. Sun and C. Y. Su, *Chem. Rev.*, 2018, **118**, 8889–8935.

22 S. V. Larionov, Y. A. Bryleva, L. A. Glinskaya, V. F. Plyusnin, A. S. Kupryakov, A. M. Agafontsev, A. V. Tkachev, A. S. Bogomyakov, D. A. Piryazev and I. V. Korolkov, *Dalton Trans.*, 2017, **46**, 11440–11450.

23 I. Olszowska-Łoś, T. Ratajczyk, I. S. Pieta, A. Siejca, J. Niedziółka-Jőnsson and A. Leśniewski, *Anal. Chem.*, 2020, **92**, 15671–15678.

24 J.-C. G. Bunzli, *Acc. Chem. Res.*, 2006, **39**, 53–61.

25 F. T. Edelmann, *Coord. Chem. Rev.*, 2018, **54**, 10021–10035.

26 J.-C. G. Bunzli, *Coord. Chem. Rev.*, 2015, **293–294**, 19–47.

27 (*a*) J. Chen, Z. Y. Xie, L. Y. Meng, Z. Y. Hu, X. F. Kuang, Y. M. Xie and C. Z. Lu, *Inorg. Chem.*, 2020, **59**, 6963–6977; (*b*) S. A. Bhat and K. Iftikhar, *Dyes Pigm.*, 2020, **179**, 108383; (*c*) Z. Ahmed and K. Iftikhar, *Dalton Trans.*, 2019, **48**, 4973–4986; (*d*) L. L. L. S. Melo, G. P. Castro Jr. and S. M. C. Goncalves, *Inorg. Chem.*, 2019, **58**, 3265–3270.

28 M. Latva, H. Mukkala, C. Matachescu, J. C. Rodriguez-Ubis and J. Kanakare, *J. Lumin.*, 1997, **175**, 149–169.

29 D. Cotter, S. Dodder, V. J. Klimkowski and T. A. Hopkins, *Chirality*, 2019, **31**, 301–311.

30 (*a*) M. A. Kaitlynn, D. S. Nathan and U. Gaël, *Inorg. Chem.*, 2020, **59**, 7657–7665; (*b*) D. E. Barry, J. A. Kitchen, L. Mercs, R. D. Peacock, M. Albrecht and T. Gunnlaugsson, *Dalton Trans.*, 2019, **48**, 11317–11325; (*c*) E. Kreidt, L. Arrico, F. Zinna, L. Di Bari and M. Seitz, *Chem. – Eur. J.*, 2018, **24**, 13556–13564; (*d*) S. Petoud, G. Muller, E. G. Moore, J. Xu, J. Sokolnick, J. P. Riehl, U. N. Le, S. M. Cohen and K. N. Raymond, *J. Am. Chem. Soc.*, 2007, **129**, 77–83.

31 (*a*) M. H. Cui, A. L. Liang, C. L. Gao, L. M. Zhou, T. Wu, S. M. Fang, H. P. Xiao, F. C. Li and X. L. Li, *Dalton Trans.*, 2021, **50**, 1007–1018; (*b*) M. Gorecki, L. Carpita, L. Arrico., F. Zinna and L. Di Bari, *Dalton Trans.*, 2018, **47**, 7166–7177.

32 (*a*) L. Wang, H. Xiao, L. Qu, J. T. Song, W. L. Zhou, X. G. Zhou, H. F. Xiang and Z. X. Xu, *Inorg. Chem.*, 2021, **60**, 13557–13566; (*b*) P. R. Xue, X. Wang, W. J. Wang, J. Y. Zhang, Z. J. Wang, J. B. Jin, C. Zheng, P. Li, G. H. Xie and R. F. Chen, *ACS Appl. Mater. Interfaces*, 2021, **13**, 47826–47834.

33 G. R. Fu, L. Liu, W. T. Li, Y. N. He, T. Z. Miao, X. Q. Lü and H. S. He, *Adv. Opt. Mater.*, 2019, **7**, 1900776.

34 (*a*) J. X. Liu, B. W. Wang, Y. Sun, X. Q. Lü, G. R. Fu, L. Liu and W.-Y. Wong, *J. Mater. Chem. C*, 2022, **10**, 11175–11180; (*b*) J. X. Liu, W. T. Li, B. W. Wang, Y. N. He, T. Z. Miao, X. Q. Lü and G. R. Fu, *J. Lumin.*, 2020, **221**, 117054; (*c*) J. X. Liu, W. T. Li, B. W. Wang, M. F. Tan, Y. N. He, T. Z. Miao, X. Q. Lü, G. R. Fu and H. S. He, *Opt. Mater.*, 2020, **107**, 109936; (*d*) R. P. Deng, L. Zhou, M. X. Song, Z. M. Hao and H. J. Zhang, *Sci. Adv. Mater.*, 2013, **5**, 1556–1562.

35 Y. N. He, L. Liu, G. R. Fu, W. T. Li, X. Q. Lü, H. S. He and W.-Y. Wong, *J. Mater. Chem. C*, 2019, **7**, 4800–4807.